1994

NASA/ASEE SUMMER FACULTY FELLOWSHIP PROGRAM

MARSHALL SPACE FLIGHT CENTER
THE UNIVERSITY OF ALABAMA

CRACKING CHARACTERISTICS OF A HABITABLE MODULE PRESSURE WALL FOLLOWING ORBITAL DEBRIS PENETRATION

Prepared By: William P. Schonberg, Ph.D.

Academic Rank: Associate Professor

Institution and Department: The University of Alabama in Huntsville
Department of Civil & Environmental Engineering

NASA/MSFC:

Laboratory: Structures and Dynamics
Division: Structural Design
Branch: Structural Development

MSFC Colleague: Dr. Joel Williamsen

INTRODUCTION

All long-duration spacecraft in low-earth-orbit are subject to high speed impacts by meteoroids and pieces of orbital debris. The threat of damage from such impacts is a significant design consideration in the development of long duration earth-orbiting spacecraft. This report presents the results of a study whose objective was develop an empirical model to predict the magnitudes of the various cracking and through-hole creation phenomena accompanying a habitable module penetration. The significance of the work performed is that the model predictions can be fed directly into a survivability analysis (see, e.g. [1,2]) to determine whether or not module unzipping would occur under a specific set of impact conditions. The likelihood of module unzipping over a structure's lifetime can also be determined in such an analysis. In addition, effective hole size predictions can be used as part of a survivability analysis to determine the time available for module evacuation prior to the onset of incapacitation due to air loss. Some of the phenomena considered include maximum petal length, maximum tip-to-tip crack distance, depth of petal deformation, number of cracks formed, orientation of the maximum tip-to-tip distance with respect to the inner wall grain direction, and the effective inner wall hole diameter.

EXPERIMENTAL SET-UP AND DATA

Figure 1 shows the normal impact (i.e. θ=0) of a dual-wall structure impacted by a spherical projectile. A total of 105 high speed impact tests were conducted at the NASA/MSFC Space Debris Simulation Facility [3]. To simulate the presence of thermal insulation in the spacecraft wall, a blanket of multi-layer insulation (MLI) was inserted between the bumper and inner wall. The witness plates behind the inner wall are used to characterize the lethality of the debris exiting the inner wall in the event of inner wall perforation.

$4.75 < D_p < 11.12$ mm
$2.9 < V_p < 7.4$ km/sec
$0 < \theta < 75$ deg
$4.32 < S < 15.24$ cm
$S_2/S = 0.23, 0.50, 0.94$
$0.81 < t_s < 2.03$ mm
$2.03 < t_w < 4.83$ mm
t_{wp}=0.51, 1.02 mm

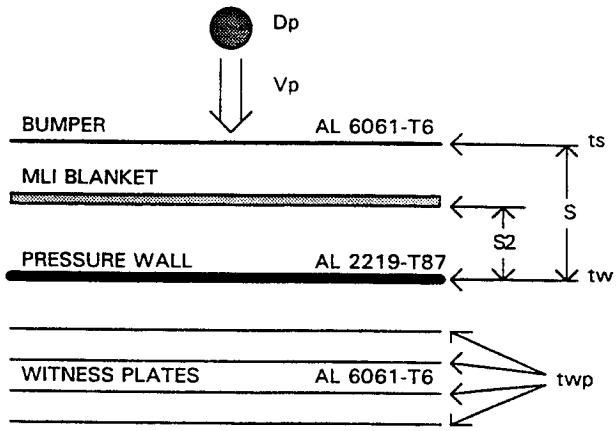

Figure 1. Hypervelocity Impact of a Generic Dual-Wall Structure

EMPIRICAL PREDICTOR EQUATIONS

Equations (1-19) are the result of a multiple linear regression analysis performed on the data; Tables 1-3 provide corresponding average errors (in percent) between actual data and regression equation predictions, standard deviations of the errors (also in percent), and correlation

coefficients. In equations (1-19), $C_w=\sqrt{(E_w/\rho_w)}$ is the speed of sound in the pressure wall material. In equation (7), the quantity $\theta_{tt}-\theta_{gr}$ denotes the orientation of the max tip-to-tip crack distance with respect to the orientation of the pressure wall grain direction. In equations (8-19), N_{kl} refers to the number of kapton layers in the MLI blanket.

MLI On The Pressure Wall, Normal and Oblique Impact, Unstressed Pressure Walls

Effective Hole Diameter

$$D_h / D_p = 5.8067(V_p / C_w)^{0.6155}(t_b / D_p)^{-0.6274}(S/D_p)^{-0.5953}(t_w / D_p)^{-0.0601}\cos^{2.1245}\theta \quad (1)$$

Maximum Petal Length

$$L_{cm} / D_p = 2.8014(V_p / C_w)^{1.7544}(t_b / D_p)^{-0.2247}(S/D_p)^{-0.4759}(t_w / D_p)^{-2.0642}\cos^{2.9966}\theta \quad (2)$$

Maximum Tip-to-Tip Distance

$$L_{tt} / D_p = 10.879(V_p / C_w)^{1.8626}(t_b / D_p)^{-0.9733}(S/D_p)^{-0.9040}(t_w / D_p)^{-0.9542}\cos^{3.6414}\theta \quad (3)$$

Depth of Petal Deformation

$$d_{pt} / t_w = 0.4815(V_p / C_w)^{1.0036}(t_b / D_p)^{-0.6534}(S/D_p)^{-1.1993}(t_w / D_p)^{-4.8489}\cos^{2.6228}\theta \quad (4)$$

Number of Cracks

$$N_{cr} = 7.7852(V_p / C_w)^{1.5215}(t_b / D_p)^{-0.8364}(S/D_p)^{-0.5892}(t_w / D_p)^{0.5680}\cos^{1.1995}\theta \quad (5)$$

Number of Perforated 0.51 mm (0.020 in.) Witness Plates

$$1+N_{wp} = 2.6460(V_p / C_w)^{1.0061}(t_b / D_p)^{-0.7948}(S/D_p)^{-0.6114}(t_w / D_p)^{0.1398}\cos^{-0.8025}\theta \quad (6)$$

Orientation of Max Tip-to-Tip Distance

$$1+\tan(\theta_{tt}-\theta_{gr}) = 0.9923(V_p / C_w)^{-0.4292}(t_b / D_p)^{-0.05545}(S/D_p)^{-0.01039}(t_w / D_p)^{-0.1486}\cos^{-0.1305}\theta \quad (7)$$

Table 1. Statistical Information for Equations 1-7

Equation No.	No. of Tests	Average Error (%)	Standard Deviation (%)	Correlation Coefficient (R^2)
(1)	74	5.93	34.59	0.71
(2)	50	5.48	34.54	0.81
(3)	50	6.68	38.52	0.86
(4)	26	2.47	23.25	0.88
(5)	47	2.57	22.96	0.67
(6)	34	3.69	28.39	0.75
(7)	42	0.19	6.27	0.74

MLI Off The Pressure Wall, Normal Impact, Unstressed Pressure Walls

Effective Hole Diameter

$$D_h / D_p = 3.0325x10^{-15}(V_p / C_w)^{1.7614}(t_b / D_p)^{-6.9854}(S_2 / S)^{1.6062}(N_{kl} / 30)^{0.7160}(t_w / D_p)^{-8.2895}(S / D_p)^{6.1144} \quad (8)$$

Maximum Petal Length

$$L_{cm} / D_p = 1.3202x10^{-8}(V_p / C_w)^{1.0708}(t_b / D_p)^{-1.4767}(S_2 / S)^{-0.4639}(N_{kl} / 30)^{0.1456}(t_w / D_p)^{-5.3054}(S / D_p)^{4.7029} \quad (9)$$

Maximum Tip-to-Tip Distance

$$L_{tt} / D_p = 4.2440x10^{-8}(V_p / C_w)^{0.9314}(t_b / D_p)^{-1.3902}(S_2 / S)^{-0.7480}(N_{kl} / 30)^{0.2337}(t_w / D_p)^{-5.2516}(S / D_p)^{4.5715} \quad (10)$$

Depth of Petal Deformation

$$d_{pt} / t_w = 4.0125x10^{-8}(V_p / C_w)^{1.6275}(t_b / D_p)^{-1.6092}(S_2 / S)^{-0.3884}(N_{kl} / 30)^{-1.1108}(t_w / D_p)^{-5.7128}(S / D_p)^{3.8105} \quad (11)$$

Number of Cracks

$$N_{cr} = 3.3609x10^{-3}(V_p / C_w)^{0.5492}(t_b / D_p)^{-0.5330}(S_2 / S)^{-0.1374}(N_{kl} / 30)^{-0.06364}(t_w / D_p)^{-2.1578}(S / D_p)^{1.6227} \quad (12)$$

Number of Perforated Witness Plates

$$1 + t_{wp}N_{wp} = 0.6902(V_p / C_w)^{0.05889}(t_b / D_p)^{-0.1442}(S_2 / S)^{0.03125}(N_{kl} / 30)^{0.02083}(t_w / D_p)^{-0.07840}(S / D_p)^{0.04118} \quad (13)$$

Table 2. Statistical Information for Equations 8-13

Equation No.	No. of Tests	Average Error (%)	Standard Deviation (%)	Correlation Coefficient (R^2)
(8)	23	4.49	29.98	0.89
(9)	23	3.51	27.08	0.73
(10)	23	4.51	31.31	0.70
(11)	23	5.37	34.06	0.81
(12)	23	1.27	16.99	0.64
(13)	23	0.02	1.80	0.78

MLI Off The Pressure Wall, Oblique Impact, Unstressed Pressure Walls

Effective Hole Diameter

$$D_h / D_p = 3.8204x10^{-4}(V_p / C_w)^{0.3675}(t_b / D_p)^{-1.9899}(S_2 / S)^{-8.7042}(N_{kl} / 30)^{14.77}(t_w / D_p)^{-1.6684}(S / D_p)^{1.4838}\cos^{1.2267}\theta \quad (14)$$

Maximum Petal Length

$$L_{cm} / D_p = 247.6(V_p / C_w)^{1.4212}(t_b / D_p)^{0.8384}(S_2 / S)^{-2.4893}(t_w / D_p)^{0.1953}(S / D_p)^{-2.0912}\cos^{0.8878}\theta \quad (15)$$

Maximum Tip-to-Tip Distance

$$L_{tt} / D_p = 823.36(V_p / C_w)^{4.9848}(t_b / D_p)^{0.8501}(S_2 / S)^{0.6084}(t_w / D_p)^{-1.7837}(S / D_p)^{-1.8892}\cos^{0.9630}\theta \quad (16)$$

Depth of Petal Deformation

$$d_{pt} / t_w = 5.6351x10^{4}(V_p / C_w)^{-1.6074}(t_b / D_p)^{3.6979}(S_2 / S)^{-3.2146}(t_w / D_p)^{-1.2269}(S / D_p)^{-2.7819}\cos^{-0.2215}\theta \quad (17)$$

Number of Cracks ($6.3<V<6.5$ km/s, $t_b=1.01$ mm, $t_w=2.03$ mm, $S=4.32$ cm, $S_2/S=0.5$ ONLY)

$$N_{cr} = 20.604(V_p / C_w)^{0.5726}(S / D_p)^{-1.3485}\cos^{-0.4642}\theta \quad (18)$$

Number of Perforated Witness Plates

$$1 + t_{wp}N_{wp} = 0.339(V_p / C_w)^{0.9278}(t_b / D_p)^{-0.1005}(S_2 / S)^{-0.2958}(t_w / D_p)^{-0.1803}(S / D_p)^{0.1754}\cos^{0.0774}\theta \quad (19)$$

Table 3. Statistical Information for Equations 14-19

Equation No.	No. of Tests	Average Error (%)	Standard Deviation (%)	Correlation Coefficient (R^2)
(14)	38	5.50	34.96	0.79
(15)	17	4.97	35.86	0.90
(16)	17	6.81	43.45	0.85
(17)	17	1.23	15.42	0.99
(18)	6	0.72	13.54	0.78
(19)	17	0.02	2.11	0.54

COMMENTS AND OBSERVATIONS

Equations (1-19) were applied to the impact of a dual-wall system with a 1.6 mm (0.063 in.) thick bumper and a 3.18 mm (0.125 in.) thick pressure wall 10 cm (4.0 in.) away from the bumper. Results were generated for 6.35, 7.95, and 9.53 mm (0.250, 0.313, and 0.375 in.) spherical projectiles impacting the dual-wall system at velocities between 3 and 7.5 km/sec. Based on the results obtained, the following general observations were made regarding the effect of MLI placement on the cracking response of a Space Station module pressure wall.

For the impact of small projectiles (i.e. 6.35 mm diameter), moving the MLI away from the pressure wall to either midway in between the bumper and pressure wall or to a position just under the bumper significantly reduced the effective pressure wall hole diameter and the extent of pressure wall cracking damage (i.e. smaller petals and crack lengths, smaller effective hole diameters, smaller petal deformation depths, fewer petals, and fewer perforated witness plates). However, for the impact of large projectiles (i.e. 9.53 mm diameter), moving the MLI away from the pressure wall did not always reduce all forms of pressure wall damage. While moving the

MLI off the pressure wall did result in smaller petals, crack lengths, and petal deformation depths, it was found that placing the MLI either midway in between the bumper and the pressure wall or near the bumper resulted in more petals, more perforated witness plates, and larger effective hole diameters (especially when the MLI was near the bumper).

Apparently, moving the MLI off the pressure wall reduces the impulsive loading of the MLI that is delivered to the pressure wall. This reduces the crack lengths and petal deformation depths. However, moving the MLI off the pressure wall also reduces its ability to trap individual debris cloud particles, especially for large projectile impacts. When the projectile is small, the energy of the debris cloud striking the MLI is relatively low. Hence, in this case the MLI is still able to trap individual debris cloud particles and produce an overall reduction in pressure wall damage. However, when the original projectile is large, the debris cloud is highly energetic. When the MLI is near the bumper, the debris cloud is still in a relatively compact state when it encounters the MLI. In such a case, the MLI is unable to trap any of the debris cloud particles and the effective hole diameter can be rather large.

CONCLUSIONS AND RECOMMENDATIONS

Based on the results obtained, it is concluded that, in most cases, moving the MLI off the pressure wall has the effect of decreasing the effective pressure wall hole diameter and the extent of pressure wall cracking damage following a pressure wall perforation. It also appears that the optimum position for the MLI is midway between the pressure wall and the bumper. This conclusion reinforces that conclusions made in two previous studies of the effect of MLI placement on dual-wall system response to high speed particle impact [4,5]. It is recommended that additional work be performed to determine the effect of module curvature on the nature and extent of pressure wall cracking following a perforation. Crack limit curves also need to be developed to define the onset of critical cracking as a function of geometry and imact conditions. .

REFERENCES

1. Williamsen, J.E., Vulnerability of Manned Spacecraft to Crew Loss from Orbital Debris Penetration, NASA-TM-108452, Marshall Space Flight Center, Alabama, 1994.

2. Micrometeoroid and Orbital Debris Induced Catastrophic Failure Prediction Methods, Space Station Freedom Program Office, Report No. GSS-40.05-RPT-6-003, Reston, Virginia, 1994.

3. Taylor, R.A., "A Space Debris Simulation Facility for Materials Evaluation", *SAMPE Quarterly*, Vol. 18, 1987, pp. 28-34.

4. Jolly, W.H. and Williamsen, J.E., "Ballistic Limit Curve Regression for Freedom Station Orbital Debris Shielding", AIAA Space Programs and Technologies Conference, Paper No. 92-1463, Huntsville, Alabama, 1992.

5. Schonberg, W.P., "Effect of Multi-Layer Thermal Insulation Thickness and Location on the Hypervelocity Impact Response of Dual-Wall Structures", *Acta Astronautica*, in press, 1994.